The High Magnetic Coupling Passive Loop: a steady-state and transient analysis of the thermal behavior

Aldo Canova, Fabio Freschi, Luca Giaccone*, and Alessandra Guerrisi
Politecnico di Torino, Dipartimento Energia,
corso Duca Degli Abruzzi, 24 - 10129 Torino

January 30, 2012

Abstract

This paper deals with a new concept of technology for the mitigation of the magnetic field produced by underground power lines called "High Magnetic Coupling Passive Loop" (HMCPL). The working principle of this technique is the creation of a current with the same amplitude but opposite phase for each source conductor, in order to nullify the magnetic field in a specified region. Since the number of thermal sources in the shielding region is roughy doubled, the aim of the paper is the investigation of the thermal behavior of HMCPL directly buried in the ground, both in transient and in steady-state conditions. The study is carried out with simulations in order to verify any possible configurations of the shield. Results confirm that HMCPL is a safe technology which does not modify the thermal behavior of the power line.

Mitigation; Magnetic field; Thermal analysis; Power cables

*Politecnico di Torino, Dipartimento Energia, corso Duca Degli Abruzzi, 24 - 10129 Torino, Italy (luca.giaccone@polito.it)

Nomenclature

a	distance between source cables (m)
c	specific heat (J/kg/K)
d	height of the volume with thermal conductivity k' (m)
h	convection coefficient $\left(\mathrm{W/m^2/K}\right)$
I_z	ampacity (A)
k	thermal conductivity (W/m/K)
k_g	thermal conductivity of the ground (W/m/K)
k'	thermal conductivity of the soil surrounding the power cables (W/m/K)
q	volume heat generation $\left(\mathrm{W/m^3}\right)$
t_{90}	time limit (days)
θ	temperature (K)
θ_{steady}	temperature in steady-state condition (K)
θ_∞	reference temperature in the FEM analysis (K)
ρ	density $\left(\mathrm{kg/m^3}\right)$
τ	time constant (days)

1 Introduction

Electromagnetic pollution is an open subject because of the possible effects on human health and the electromagnetic compatibility issue. These are the reasons why magnetic field mitigation is an active field of research [1], [2]. A special type of conductive shield is represented by the passive loops. These shields are made of electrical conductors (typically the same electric cables used for transport and distribution) connected to each other in order to create closed loops. The working principle is based on electromagnetic induction: time varying magnetic fields, produced by AC currents, induce eddy currents in conductive loops and consequently they constitute an additional field source which modifies and attempts to reduce the main magnetic field produced by the sources. This kind of shield is used both for buried cable and overhead power lines [3]. In previous papers, a new concept of passive loop called the High Magnetic Coupling Passive Loop (HMCPL) was introduced along with a description of its magnetic performances [4], [5], [6], [7], [8]. HMCPL technology is very suitable for magnetic field mitigation of the junction. The cables are usually arranged in trefoil configuration but, when they need to be joined, the flat configuration has to be adopted because the joint needs larger spaces [8], a simple representation is shown in Fig. 1. It is worth noting that the use of the flat configuration leads to a higher magnetic field at ground level as shown in Fig. 2. This is the reason why the junction zone might need to be shielded.

To give a short overview of the HMCPL technique, the base layout is the one which associates a shielding conductor to each power cable as shown in Fig. 3. The magnetic cores allow the induction of currents inside the shielding circuit which are equal, to a first approximation, in amplitude but in phase opposition with respect to the source currents, so that the local magnetic field vanishes.

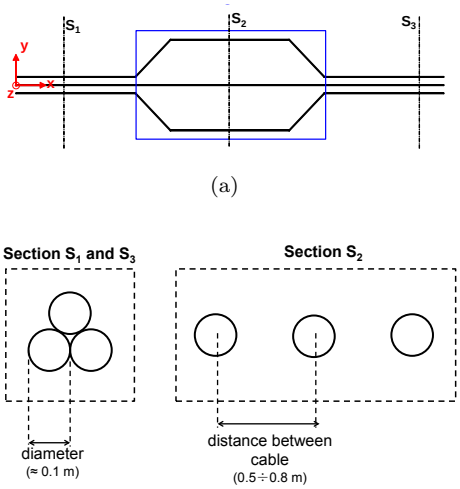

Figure 1: Classical layout of the junction zone (a) Cable sections (b)

When it is not possible to reach the power lines due to practical or technical problems (e.g. the need to shield an existing power line or shield a power line arranged in a trefoil configuration) the HMCPL could be used with a layout that employs a non-unitary coupling [4]. In this layout the shielding conductors are placed far from the source and they carry a current which is determined by a proper transformer ratio [4]. Therefore the design of this layout needs to be optimized to determine the position of the shielding conductors and the value of the transformer ratio [4].

The use of HMCPL technology imposes the introduction of a new set of conductors and, consequently, new joule losses. Therefore a thermal analysis of the system is unavoidable in order to clarify whether the installation of a HMCPL leads to an ampacity derating of the power line or not.

In this paper the thermal behavior of a power line which employs HMCPL directly buried in the ground is carefully analyzed by means of steady-state, transient analysis and measurements.

2 Thermal design of a power line

The thermal design of power system components is a challenging task. Several studies on power lines can be found in the Literature. The thermal equations are often analyzed by means of circuital approaches [9], [10], [11] or different numerical methods [12], [13], [14], [15], [16]. Many works consider the coupled magneto-thermal problem [9], [13], [17], [18]. In this paper, underground power cables are considered and the thermal problem is solved by means of numerical models thereby considering it as stand-alone uncoupled problem.

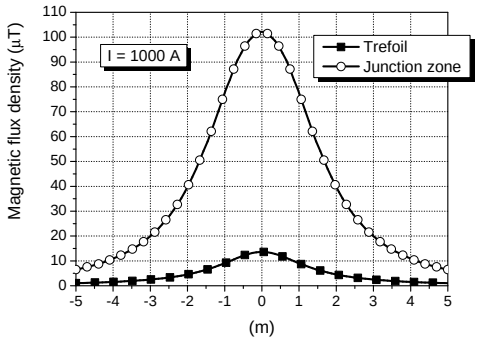

Figure 2: Magnetic induction at the ground level on a line orthogonal to the cables (trefoil and Junction zone)

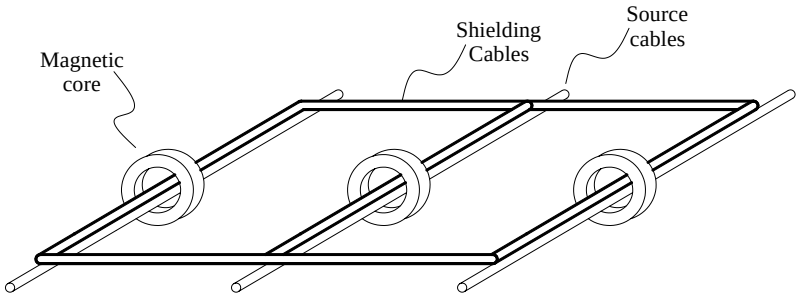

Figure 3: Geometrical layout of HMCPL with unitary coupling

The power line to be designed is arranged for most of the path in trefoil configuration and, in correspondence of the junction zone, HMCPL technology is employed. Both cases are interesting because where the power line is arranged in a trefoil configuration the cables are strongly coupled from the thermal point of view. Within the junction zone the flat configuration is used and, consequently, the cables are less stressed from the thermal point of view. On the other hand flat configuration leads to a magnetic field at ground level which exceeds the suggested limits [19]. Therefore the HMCPL is used for lowering the magnetic field and a new verification of the thermal condition in the junction zone is needed.

The thermal simulations are performed by means of DualLab which is a collection of MATLAB routines that are useful to build numerical solvers for many physical theories. The toolbox is not an all-in-one program to solve a specific field problem, but rather an environment which makes the data structure available for implementing different formulations. Users must supply the initial discretization data (i.e. points coordinates, connectivity matrix and material codes), provided by standard mesh generators, and use the provided functions for building primal and dual data structures, incidence matrices and boundary conditions [20].

For steady-state thermal problem the following equation has to be solved:

$$k\nabla^2\theta + q = 0 \tag{1}$$

where:

- k is the thermal conductivity (W/m/K);
- θ is the temperature (K);
- q is the volume heat generation (W/m^3).

In this section the power line in trefoil configuration is taken as a test case for the calibration of the model. The main parameters of the cable (represented in Fig. 4) are given by the manufacturer and they are summarized in Table 1. In this cable the "airbag layer" is employed. It is a new solution composed by extruded plastic layer that provides better mechanical protection than traditional metal armoured cable. It is designed and patented by the manufacturer and it is able to absorb the kinetic energy of a shock by plastic deformation. Finally, in Table 2 the thermal parameters of each layer are summarized.

Table 1: Main parameters of the cable

Rated Voltage	220 kV
Rated Current (Ampacity)	1400 A
Cross section	1600 mm^2
Insulation	XLPE

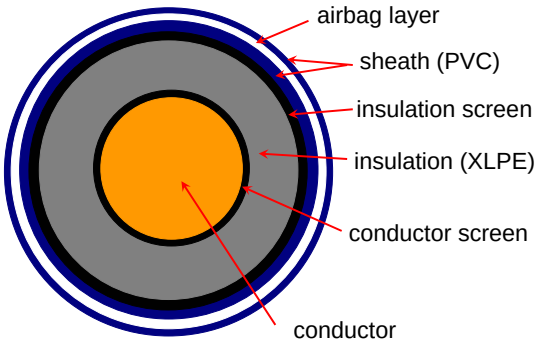

Figure 4: Main layers of the cable

TABLE 2: Thermal conductivities of layers

Layer	Thermal conductivity (W/m/K)
Conductor (Cu)	386
Cond. screen (Al)	237
Insul. (XLPE)	0.29
Insul. screen (Al)	237
Sheath. (PVC)	0.29
Airbag	0.125
Sheath. (PVC)	0.29

The cable ampacity is defined for installation 1.5 m below the ground level, therefore the FEM model to be used is represented in Fig. 5 where the volume heat generation (q) inside the cables could be computed by means of the AC resistance parameter given by the manufacturer.

Two different boundary conditions have been used: thermal convection (thermal exchange from ground to air) and null flux out of the boundary (at the end of the domain in the ground) [13], [12], [21].

With reference to Fig. 5, the thermal exchange from ground to air is modeled by the convection boundary. Hence the heat transfer coefficient h has to be defined in order to solve the problem. Defining I_z as ampacity, the current value which brings one of the trefoil conductors to the thermal limit (here considered as 90 °C), the influence of h on the ampacity has been investigated and the results are shown in Fig. 6. From the analysis of Fig. 6 it is possible to derive the value of the heat transfer coefficient which allows the (known) ampacity of the trefoil configuration to be obtained. The value of 1400 A is obtained by setting $h = 0.81$ W/m^2/K. It has to be stressed that the obtained value is conservative with reference to the ones suggested in the bibliography [13] ,[21].

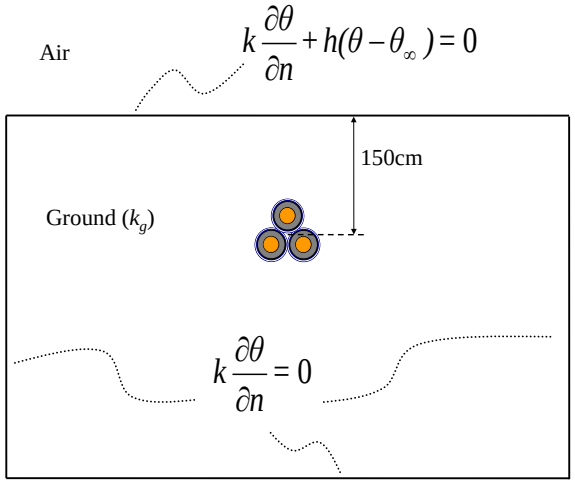

Figure 5: FEM model

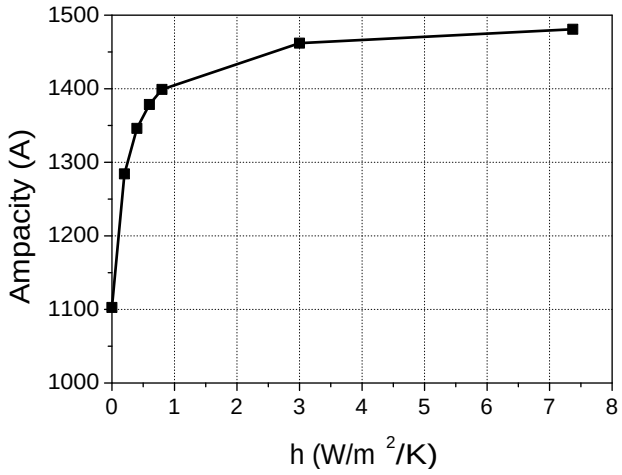

Figure 6: ampacity vs heat transfer coefficient

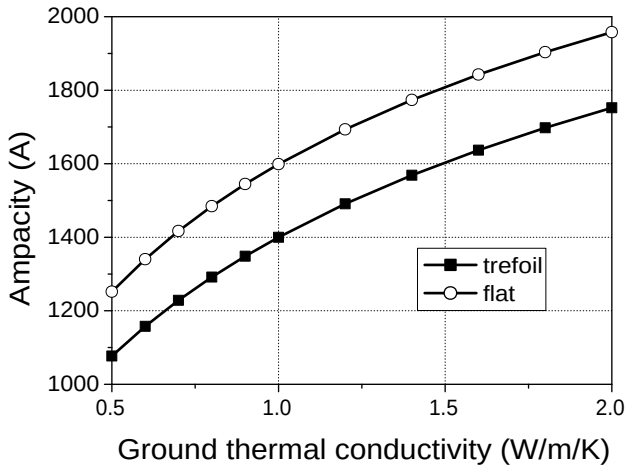

Figure 7: Ampacity vs ground thermal conductivity

2.1 Influence of the thermal conductivity of the ground on the ampacity

The standards usually suggest the use of $k_g = 1$ W/m/K for the thermal conductivity of the ground but, since this parameter is uncertain [10], [22] a preliminary analysis is aimed at investigating the influence of the thermal conductivity of the ground on the ampacity. Two different configurations have been considered: 1) trefoil configuration, 2) flat configuration (distance between conductors equal to 70 cm).

The results are summarized in Fig. 7 where it is possible to note how the thermal conductivity of the ground is a parameter with a high influence on the system ampacity. The first (obvious) consideration is that, for a given value of thermal conductivity, the flat configuration reaches the thermal limit for a higher current value than the one relative to the trefoil. In other words, the ampacity of the line has to be defined taking into account the trefoil configuration.

Finally the simulation of the flat configuration considering a thermal conductivity equal to $k_g = 1$ W/m/K and supplying the system with 1400 A (ampacity of the trefoil) has been done. The temperature profile of the system has been plotted in Fig. 8 (where the reference line for the temperature plot is represented at the top of the graph). The maximum temperature value is observed in the central conductor. Moreover, the temperature is always lower than 90 °C as expected. Therefore, the introduction in that section of higher Joule losses (introduction of the HMCPL) is allowed.

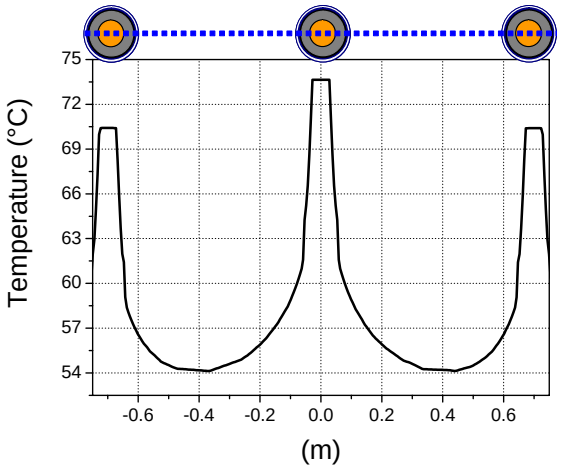

Figure 8: Temperature profile of the flat configuration along the reference line represented above the plot (parameters: $k_g = 1$ W/m/K and $I_z = 1400$ A)

3 HMCPL steady-state simulation

The introduction of the HMCPL in the junction zone has been analyzed with reference to the model shown in Fig. 9. The parameters taken into account are: cross section of the shielding cables (185 mm^2 or 240 mm^2), thermal conductivity of the trench ($k' = 1$; 1.5; 2 W/m/K), dimension of the trench ($d = 25$; 50; 100; 150 cm), distance between phases ($a = 70$; 100; 120 cm). Phase splitting technique is used to improve the shielding efficiency [8] therefore the number of the shielding cables applied to a single source cable is also taken into account as a parameter (4 or 8, Fig. 9 represents 4 cables). The combination of all the possible parameter values determines several configurations which have been simulated. In Tables 3, 4, 5 and 6 the results obtained by varying cross section, number of shielding conductors, dimension and thermal conductivity of the trench are shown (distance between phases is here considered constant to $a = 70$ cm). In these tables two particular combinations are represented: 1) when $k' = 1$ W/m/K all the ground is considered homogeneous, 2) when $d = 150$ cm the trench with different thermal conductivity is extended up to the ground boundary.

From the analysis of these tables it is possible to note that the ampacity of the system strongly depends on the thermal conductivity of the ground. Most of the configurations lead to an ampacity lower than 1400 A, this result means that the flat configuration with the HMCPL imposes a lower constraint on the ampacity with respect to the trefoil section, therefore the whole power line is subject to a derating. Only two of the analyzed configurations are feasible without imposing a derating of the system: the ones where the trench and the thermal conductivity are set to their maximum value.

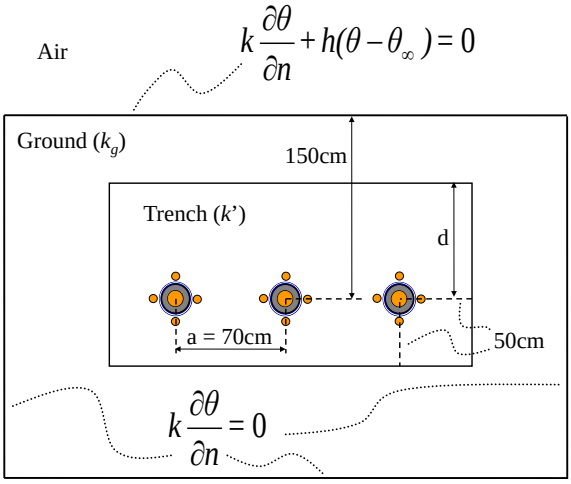

Figure 9: FEM model - introduction of the trench

TABLE 3: Ampacity

$d = 25$ cm - $a = 70$ cm			
	Thermal conductivity k'		
	1	1.5	2
4×185 mm^2	1015 A	1063 A	1091 A
4×240 mm^2	1100 A	1150 A	1180 A
8×185 mm^2	1213 A	1266 A	1298 A
8×240 mm^2	1283 A	1337 A	1370 A

It is worth noting that, even if the ampacity of the trefoil is 1400 A, usually this value does not coincide with the ampacity of the power line because along the whole span are often used/required some special cable arrangements. For instance the "horizontal directional drilling" technique is used when the power line intercepts a river or a railway path. With this technique the power cables are placed deeper than usual and the ampacity related to this section could decrease up to $1100 \div 1200$ A imposing an "a priori" derating to the power line. In this paper the value of 1400 A is taken as the worst case (from the HMCPL point of view).

The last parametric result is obtained by considering the influence of the distance between phases on the ampacity. In order to avoid a huge amount of configurations the influence of the distance is analyzed just for the configuration with ground homogeneity ($k' = 1$ W/m/K). The results are shown in Fig. 10 where it can be noted that the increment of the distance between phases is followed by an increment of the system ampacity. By normalizing the results

TABLE 4: Ampacity

$d = 50$ cm - $a = 70$ cm			
	Thermal conductivity k'		
	1	1.5	2
4×185 mm^2	1015 A	1074 A	1110 A
4×240 mm^2	1100 A	1162 A	1200 A
8×185 mm^2	1213 A	1280 A	1319 A
8×240 mm^2	1283 A	1351 A	1392 A

TABLE 5: Ampacity

$d = 100$ cm - $a = 70$ cm			
	Thermal conductivity k'		
	1	1.5	2
4×185 mm^2	1015 A	1090 A	1137 A
4×240 mm^2	1100 A	1179 A	1228 A
8×185 mm^2	1213 A	1298 A	1350 A
8×240 mm^2	1283 A	1370 A	1423 A

TABLE 6: Ampacity

$d = 150$ cm - $a = 70$ cm			
	Thermal conductivity k'		
	1	1.5	2
4×185 mm^2	1015 A	1101 A	1157 A
4×240 mm^2	1100 A	1190 A	1249 A
8×185 mm^2	1213 A	1310 A	1372 A
8×240 mm^2	1283 A	1382 A	1446 A

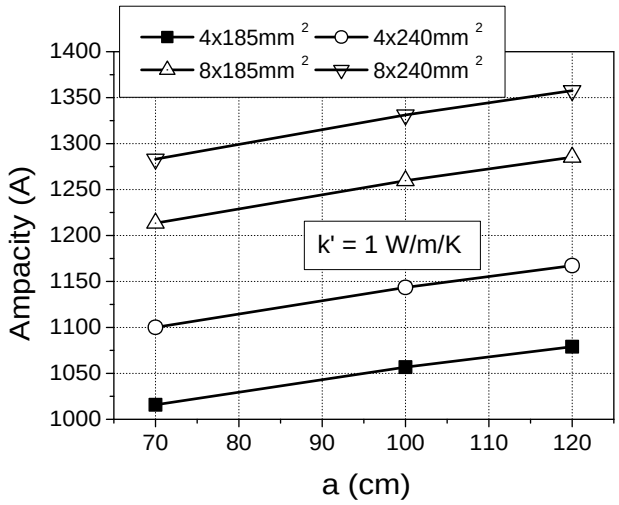

Figure 10: Ampacity vs distance between phases

of Fig. 10 it transpires (Fig. 11) that increasing the cable distance a has the same relative increase as the system ampacity, independently of the number of shielding cables per phase.

4 HMCPL Transient analysis

Even if the steady-state analysis seems to impose a derating for most of the configurations, a transient analysis is necessary in order to clarify if this derating needs to be imposed on the system or not.

In order to take into account the thermal transient the time derivative of the temperature must be added to (1), obtaining:

$$-\rho c \frac{\partial \theta}{\partial t} + k\nabla^2\theta + q = 0 \tag{2}$$

where:

- ρ is the density (kg/m^3);
- c is the specific heat (J/kg/K);
- θ is the temperature (K);
- k is the thermal conductivity (W/m/K);
- q is the volume heat generation (W/m^3).

The configurations already studied in steady-state conditions have again been analyzed in order to:

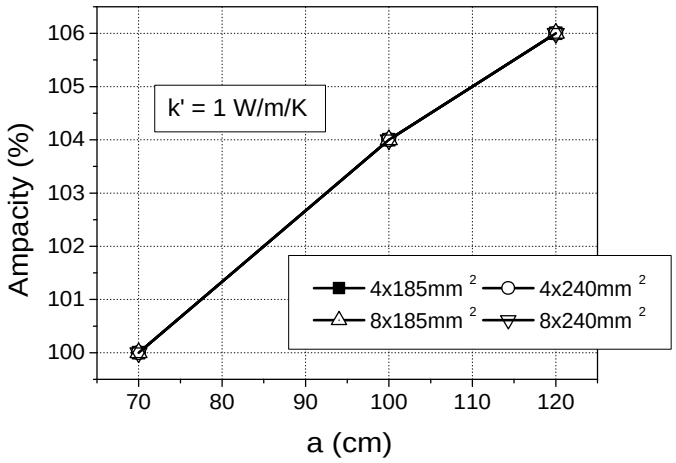

Figure 11: Ampacity vs distance between phases (percentage variation)

- calculate the thermal time constant of the system;
- calculate the "time limit" (i.e. the time needed to reach the temperature of 90 °C).

Finally, for the most critical system (configuration 4 x 185 mm^2) some simulations have been done taking into account the load profile of the power line.

4.1 Time constant calculation

In each configuration the system is supplied by a current equal to the ampacity I_z. The ampacity values have been computed in the steady-state simulations (Tables 3, 4, 5 and 6).

In Tables 7, 8, 9 and 10 the results of this transient analysis are shown. As is expected, the steady-state temperature is equal to 90 °C for all the configurations but, a very important result is that, the exponential behavior which leads to the steady-state temperature presents a time constant of about 200 days. In Fig. 12 and 13 temperature profiles at steady-state and the transient are shown for the most critical configuration: 4×185 mm^2 - $k' = 1$ W/m/K - $d = 25$ cm - $I_z = 1015$ A.

In all the simulations the average values of specific heat and density of ground are considered : $c = 1050$ J/kg/K and $\rho = 2000$ kg/m^3. When the simulations are performed with the minimum values of specific heat and density of ground ($c = 700$ J/kg/K and $\rho = 1400$ kg/m^3) [10] the time constant is halved to 100 days which is much larger than the load profile periodicity. The high value of the thermal constant time is confirmed by the bibliographic data where simulations [23] and measurements [11] lead to a transient of several days.

Table 7: Time constant

$d = 25$ cm - $a = 70$ cm				
	k' (W/m/K)	τ (days)	4τ (days)	θ_{steady} (°C)
4×185 mm^2	1	209	837	89.94
4×240 mm^2		209	837	90.02
8×185 mm^2		205	820	90.02
8×240 mm^2		192	768	90.06
4×185 mm^2	1.5	222	890	90.08
4×240 mm^2		222	890	90.06
8×185 mm^2		218	872	90.02
8×240 mm^2		203	814	90
4×185 mm^2	2	231	925	90.02
4×240 mm^2		227	907	90.05
8×185 mm^2		222	890	90.01
8×240 mm^2		209	837	90

Table 8: Time constant

$d = 50$ cm - $a = 70$ cm				
	k' (W/m/K)	τ (days)	4τ (days)	θ_{steady} (°C)
4×185 mm^2	1	209	837	89.94
4×240 mm^2		209	837	90.02
8×185 mm^2		205	820	90.02
8×240 mm^2		192	768	90.06
4×185 mm^2	1.5	222	890	89.97
4×240 mm^2		218	872	89.99
8×185 mm^2		214	855	90.08
8×240 mm^2		201	803	90.01
4×185 mm^2	2	227	907	90.04
4×240 mm^2		227	907	90.06
8×185 mm^2		222	890	90
8×240 mm^2		206	826	90.02

Table 9: Time constant

$d = 100$ cm - $a = 70$ cm				
	k' (W/m/K)	τ (days)	4τ (days)	θ_{steady} (°C)
4×185 mm^2	1	209	837	89.94
4×240 mm^2		209	837	90.02
8×185 mm^2		205	820	90.02
8×240 mm^2		192	768	90.06
4×185 mm^2	1.5	218	872	89.98
4×240 mm^2		214	855	90.01
8×185 mm^2		209	838	90.09
8×240 mm^2		198	791	90.06
4×185 mm^2	2	222	890	90.04
4×240 mm^2		218	872	90
8×185 mm^2		214	855	90.07
8×240 mm^2		201	803	90

Table 10: Time constant

$d = 150$ cm - $a = 70$ cm				
	k' (W/m/K)	τ (days)	4τ (days)	θ_{steady} (°C)
4×185 mm^2	1	209	837	89.94
4×240 mm^2		209	837	90.02
8×185 mm^2		205	820	90.02
8×240 mm^2		192	768	90.06
4×185 mm^2	1.5	214	855	90.02
4×240 mm^2		209	837	89.96
8×185 mm^2		205	820	90.08
8×240 mm^2		195	779	90.01
4×185 mm^2	2	214	855	90.04
4×240 mm^2		209	837	89.98
88×185 mm^2		205	820	90.04
8×240 mm^2		192	768	89.99

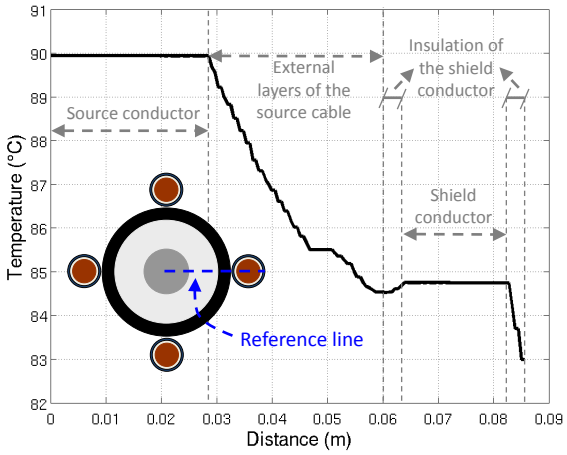

Figure 12: Steady-state solution along the reference line (4×185 mm^2 - $k' = 1$ W/m/K - $d = 25$ cm - $I_z = 1015$ A)

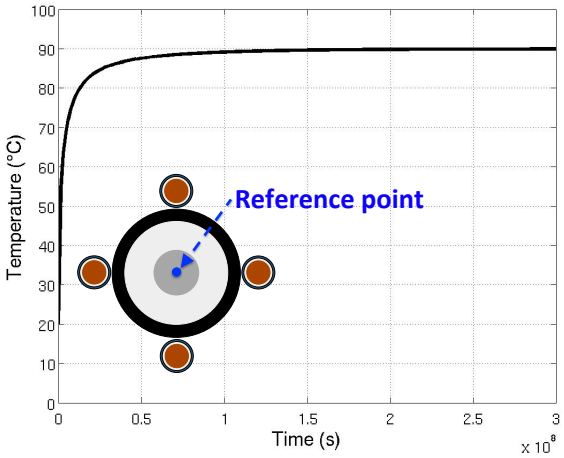

Figure 13: Transient in the central reference point (4×185 mm^2 - $k' = 1$ W/m/K - $d = 25$ cm - $I_z = 1015$ A)

TABLE 11: Time limit and steady-state temperature

$d = 25$ cm - $a = 70$ cm			
	k' (W/m/K)	t_{90} (days)	θ_{steady} (°C)
4×185 mm^2	1	15	153.1
4×240 mm^2		26	133.4
8×185 mm^2		57	113.3
8×240 mm^2		109	103.3
4×185 mm^2	1.5	24	141.6
4×240 mm^2		43	123.8
8×185 mm^2		105	105.6
8×240 mm^2		246	96.75
4×185 mm^2	2	33	135.3
4×240 mm^2		59	118.6
8×185 mm^2		157	101.5
8×240 mm^2		508	93.1

4.2 Time limit calculation

It is interesting to analyze how much time is needed to reach the limit temperature of 90 °C if the system is supplied with a higher current than its ampacity. This analysis is aimed at understanding if the derating evaluated with the steady-state analysis is really necessary or not. Therefore, each system is supplied with a current equal to 1400 A (ampacity of the trefoil configuration) and the following results are presented:

- steady-state temperature θ_{steady} of the more thermally stressed conductor (the central one);
- time limit: the time needed to reach 90 °C.

The results for each configuration are shown in Tables 11, 12, 13, 14 and Fig. 14.

In all the simulations (e.g. Fig. 15) the initial temperature is set to $\theta_0 =$ 20 °C and the source current is $I_z = 1400$ A. The time needed to reach the limit of 90 °C and the final temperature θ_{steady} depends on the number and the section of shield conductors and on the trench thermal conductivity and dimension.

4.3 Simulations with power line load profiles

In the previous simulations the system was supplied by a constant current while in the following simulations the system is supplied by a load curve. The configuration 4×185 mm^2 has been considered, with homogeneous ground (everywhere

TABLE 12: Time limit and steady-state temperature

$d = 50$ cm - $a = 70$ cm			
	k' (W/m/K)	t_{90} (days)	θ_{steady} (°C)
4×185 mm^2	1	15	153.1
4×240 mm^2		26	133.4
8×185 mm^2		57	113.3
8×240 mm^2		109	103.3
4×185 mm^2	1.5	27	138.9
4×240 mm^2		47	121.6
8×185 mm^2		120	103.8
8×240 mm^2		310	95.18
4×185 mm^2	2	38	131.4
4×240 mm^2		67	115.4
8×185 mm^2		201	98.86
8×240 mm^2		1169	90.83

TABLE 13: Time limit and steady-state temperature

$d = 100$ cm - $a = 70$ cm			
	k' (W/m/K)	t_{90} (days)	θ_{steady} (°C)
4×185 mm^2	1	15	153.1
4×240 mm^2		26	133.4
8×185 mm^2		57	113.3
8×240 mm^2		109	103.3
4×185 mm^2	1.5	29	135.4
4×240 mm^2		52	118.7
8×185 mm^2		141	101.5
8×240 mm^2		462	93.16
4×185 mm^2	2	43	126.2
4×240 mm^2		80	111
8×185 mm^2		308	95.36
8×240 mm^2		xxx	87.75

TABLE 14: Time limit and steady-state temperature

$d = 150$ cm - $a = 70$ cm			
	k' (W/m/K)	t_{90} (days)	θ_{steady} (°C)
4×185 mm^2	1	15	153.1
4×240 mm^2		26	133.4
8×185 mm^2		57	113.3
8×240 mm^2		109	103.3
4×185 mm^2	1.5	29	133.2
4×240 mm^2		54	116.8
8×185 mm^2		157	100
8×240 mm^2		676	91.84
4×185 mm^2	2	46	122.6
4×240 mm^2		89	107.9
8×185 mm^2		484	92.92
8×240 mm^2		xxx	85.61

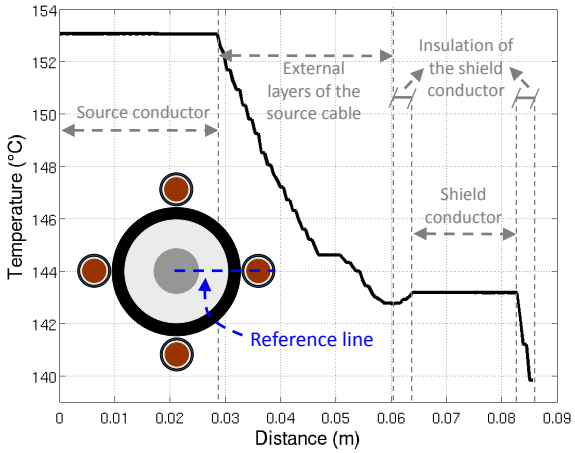

Figure 14: Steady-state solution along the reference line (4×185 mm^2 - $k' = 1$ W/m/K - $d = 25$ cm - $I_z = 1400$ A)

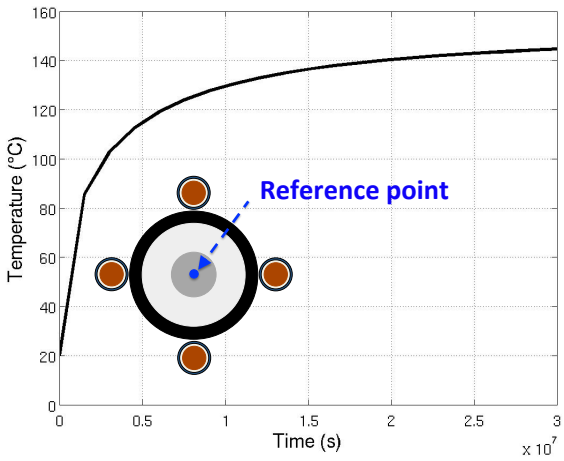

Figure 15: Transient in the central reference point (4×185 mm^2 - $k' = 1$ W/m/K - $d = 25$ cm - $I_z = 1400$ A)

$k' = 1$ W/m/K). The actual load profile of a power line was measured over one day and, for the simulations, it was scaled in order to keep the shape but obtaining a peak value of 1400 A, see Fig. 16.

The initial temperature θ_0 of these simulations is the temperature θ_{steady} obtained by simulating the system supplied with a current equal to the r.m.s. value of the considered waveform.

By supplying the system with the reshaped load curve the temperature obtained at steady-state reaches a peak of about 94 °C; whereas if the system is supplied with a constant current equal to 1400 A the temperature obtained is higher: 153.1 °C (Fig. 17). Moreover, it is important to underline that 94 °C is the peak of the obtained temperature. At steady-state for most of the time the temperature of the system is lower than 90 °C as shown in Fig. 17.

Finally, for the same configuration (4×185 mm^2), some simulations have been done considering the reshaped load profile and varying the thermal conductivity of ground in the trench. Once again, by increasing the value of thermal conductivity of the ground in the trench, the maximum temperature reached is reduced. In the cases of Fig. 18 and 19 ($k' = 1.5$ and 2 W/m/K respectively) the limit temperature of 90 °C is not violated.

5 Effect of the ending connections

The ending connections of the HMCPL system must be taken into account during the design of the shield. To maximize the magnetic performances the ending connections should be placed as close as possible to the trefoil conjunction but, on the other hand the higher vicinity of the group of cables can create a thermal

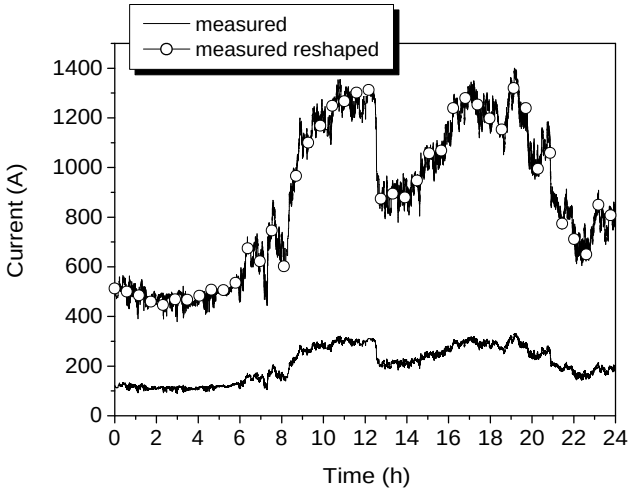

Figure 16: Measured load profile and reshaped load profile

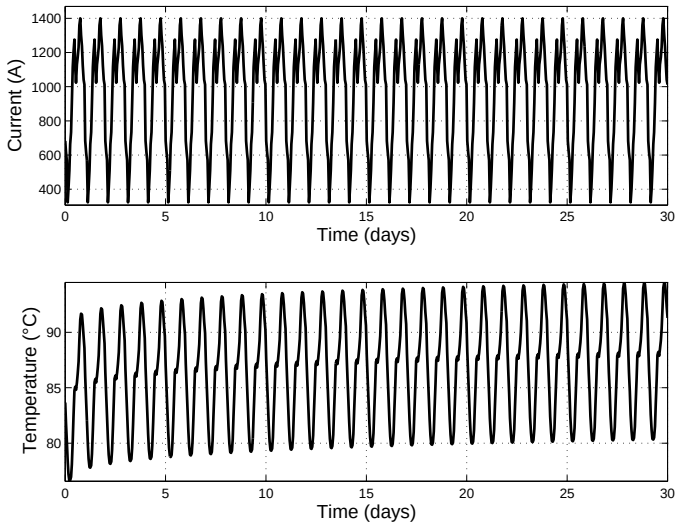

Figure 17: Reshaped load curve (configuration 4×185 mm^2 - $k' = 1$ W/m/K - $d = 25$ cm)

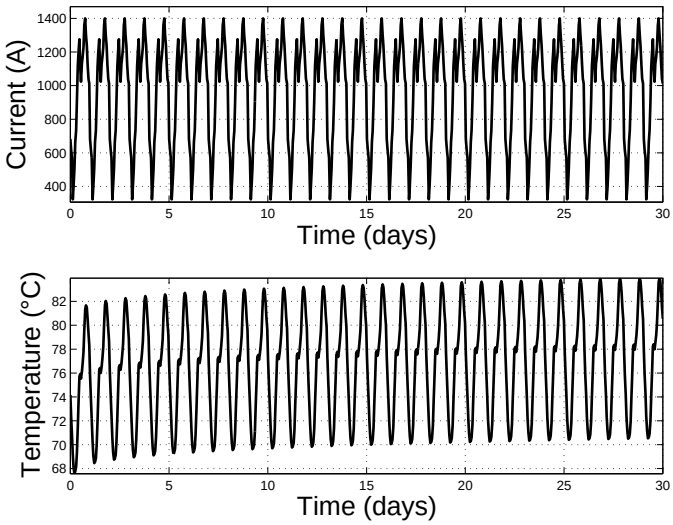

Figure 18: Reshaped load curve (configuration 4×185 mm^2 - $k' = 1.5$ W/m/K - $d = 150$ cm)

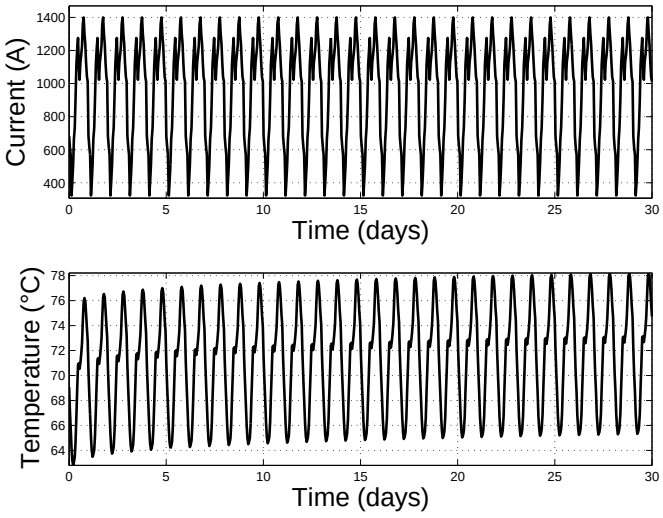

Figure 19: Reshaped load curve (configuration 4×185 mm^2 - $k' = 2$ W/m/K - $d = 150$ cm)

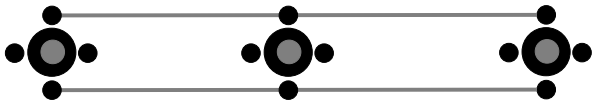

(a)

(b)

Figure 20: Layout of the ending connections (a) Realization of the ending connection (b)

"hot spot". In order to investigate the influence of the ending connections on the global thermal behavior a 2D model is not sufficient: it is a good approximation (at least conservative) in order to design the HMCPL in the center of the junction zone but it is not representative for the analysis of the edge effect (i.e. when the shielding conductors reach the ending connection). Therefore a 3D model has been created and the analysis is performed for a steady-state configuration designed in order to keep the temperature below the defined limit (90 °C) in all the system. In the 3D analysis the distance between source cables and the thermal conductivity of the ground are constant and equal to 0.7 m and 1 W/m/K respectively. Due to symmetry reason the whole domain can be reduced to 1/4 of the domain by using the proper boundary conditions. It has to be stressed that the final realization of the HMCPL takes into account 4 ending connections because it can be realized by two subsystems: six lower cables and six upper cables connected at both ends with a short circuit as represented in Fig. 20(a) [24]. The decoupling of the HMCPL in two subsystems does not affect the magnetic behavior and, moreover, it allows to employ a final ending connection realized as shown in Fig. 20(b). It is made by a flexible cable with three conductive plates where it is possible to fix six cable lugs. Moreover it is possible to use an epoxy resin which assures the protection against corrosion.

The analyzed domain is represented in Fig. 21. The meshed domain and an example of the total thermal field are represented in Fig. 22.

By means of a 3D model it is possible to plot the temperature profile along three interesting lines: the first one is centered with respect to the junction zone, the second one is placed prior to the conjunction of the power cables and the third one is located exactly between two ending connection. The three lines are represented in Fig. 23 and the results are summarized in Fig. 24.

From the analysis of Fig. 24 it is possible to observe that the temperature for the central conductor is always decreasing going from the center of the junction zone to the trefoil arrangement (comparison of "line 1", "line 2" and "line 3" in the coordinate equal to zero). All the lines, after an initial decrease, present

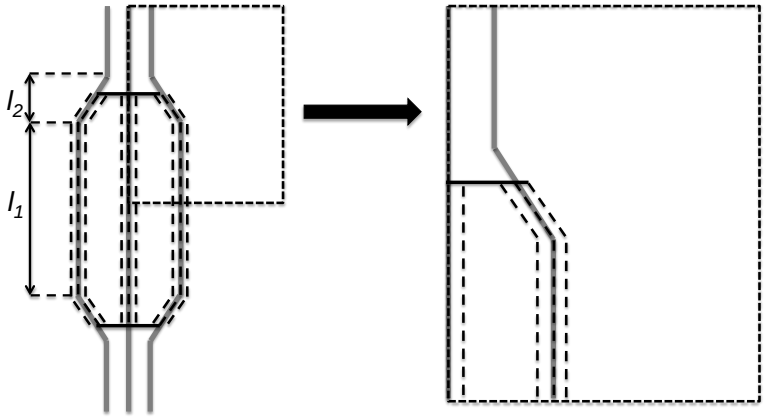

Figure 21: Junction zone: complete domain (left) 1/4 of the domain (right)

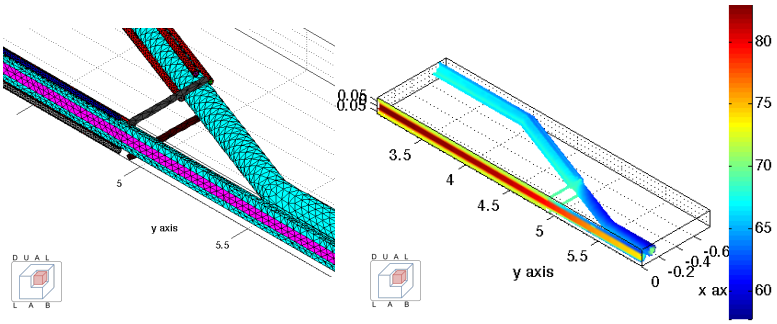

Figure 22: Junction zone: meshed domain (left) thermal field (right)

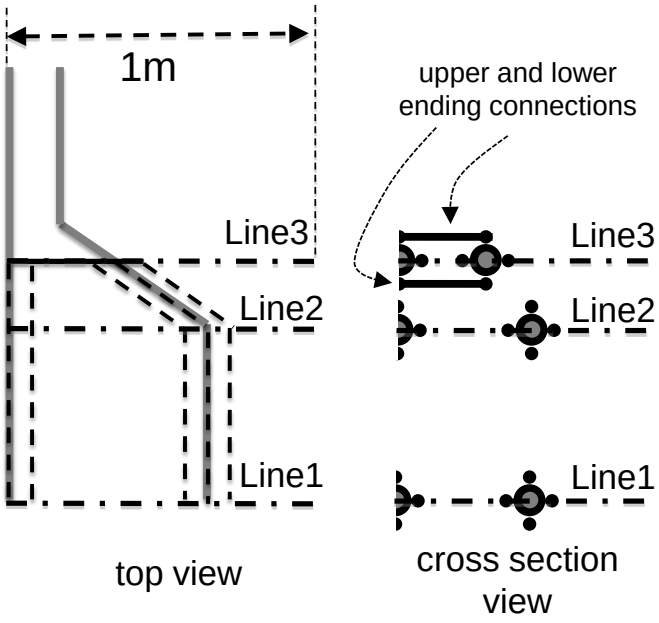

Figure 23: Reference paths for the temperature plot

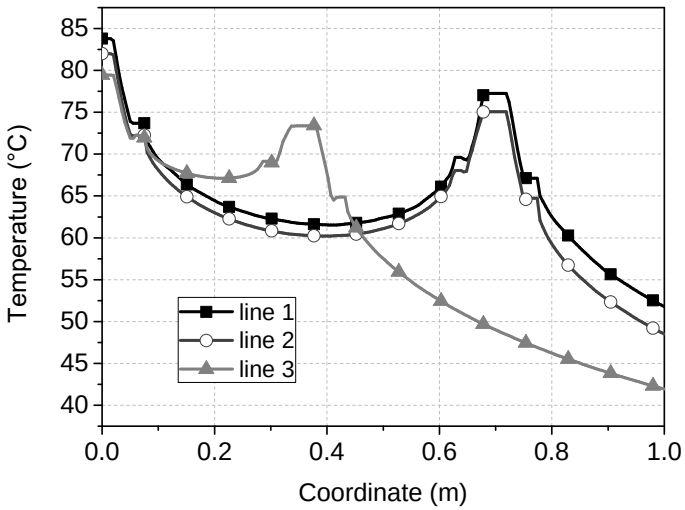

Figure 24: Temperature plot

a second temperature peak that corresponds to the lateral power cables. The peak of the "line 3" (triangle symbol) is not located in the same place of the other two curves because the "line 3" intercepts the lateral cables in a different position with respect to the previous reference lines. Peak temperature along "line 3" is lower than that along "line 1" because the volume heat generation due to shielding cables is limited to the part closed to the junction zone. Finally, the temperature of the lateral cable is (once again) decreasing going from the center of the junction zone to the trefoil arrangement, moreover, the temperature of the lateral cables is lower than the one of the central cable.

In conclusion, the vicinity of the shielding cables close to the ending connection does not imply an increase of temperature that leads to a thermal derating.

6 Conclusions

The main objective of this paper is to define a procedure which allows the HMCPL system to be designed without affecting the ampacity of the system.

When the HMCPL is applied to a flat configuration the best magnetic performances are obtained by placing the shielding cables very close to the power lines, therefore a possible derating of the system has to be taken into account. In this paper several parametric simulations have been performed to obtain information about the influence of the ground thermal conductivity and the distance between phases on the system ampacity. The thermal conductivity of the ground plays a key role in the ampacity of the system (defined in steady state condition) and, unfortunately, is also a parameter which can be known with low accuracy. The increase of the distance between phases (up to a feasible value) allows higher ampacity values to be obtained which do not depend on the set of shielding cables.

As a general conclusion, the insertion of the shielding cables reduces the ampacity of the power cables below the one of the trefoil configuration, with the exception of using a high conductivity fill for the trench where the shielding cables are located. It is worth noting that the overall effect of the HMCPL on the trefoil ampacity could be negligible when compared with other unavoidable bottlenecks along the power line path.

A further improvement of the analysis has been carried out by considering the thermal transient. Even if many configurations are subject to derating if analyzed in steady-state condition, the transient analysis shows how the thermal time constant of the system is higher than the variation of the load profile over 24 hours. This means that a huge amount of time is needed to achieve the actual steady-state temperature. This result is proven by simulating the most critical configuration based on a load profile with higher peaks than the computed ampacity and obtaining a temperature trend which is not as critical as foreseen by the steady-state simulation.

Finally, a 3D model of the junction zone with the HMCPL system has been taken into account for the investigation of the thermal behavior of the ending connections concluding that, even if the power cables are closer and the ending

connection is another thermal source the temperature is not critical if the system is well designed.

References

[1] Review of the scientific evidence for limiting exposure to electromagnetic fields (0-300 GHz), Tech. Rep. Vol. 15 N.3, National Radiological Protection Board (2004).
URL `www.nrpb.org [January 30, 2012]`

[2] Mitigation techniques of power frequency magnetic fields originated from electric power systems, Tech. Rep. Worging group C4.204, International Council on Large Electric Systems (CIGRÉ) (2009, ISBN: 978-2-85873-060-5).

[3] B. Shperling, L. Menemenlis-Hopkins, B. Fardanesh, B. Clairmont, D. Child, Reduction of magnetic fields from transmission lines using passive loops, in: Cigré 1996 - Paper 36-103, 1996.

[4] A. Canova, L. Giaccone, Optimal design of high magnetic coupling passive loop for power lines field mitigation, COMPEL 28 (2009) 1294–1308.

[5] A. Canova, L. Giaccone, Magnetic field mitigation of power cable by high magnetic coupling passive loop, in: The 20th International Conference and Exhibition on Electricity Distribution, CIRED 2009., Prague, Czech Republic, 8-11 June 2009.

[6] A. Canova, L. Giaccone, Sistema di schermatura passiva di tipo magliato e conduttivo ad elevato accoppiamento magnetico, Patent n. TO2008A000176 (2008).

[7] A. Canova, L. Giaccone, Passive shielding system of a meshed and conductive type with high magnetic coupling passive loop, PCT/IB2009/000445 (2009).

[8] A. Canova, L. Giaccone, A novel technology for magnetic-field mitigation: High magnetic coupling passive loop, IEEE Transactions on Power Delivery Vol. 26 (N. 3) (2011) 1625 – 1633.

[9] T. L. Jones, The calculation of cable parameters using combined thermal and electrical circuit models, IEEE Transactions on Power Delivery 4 (3) (1989) 1529–1540.

[10] D. Villaci, A. Vaccaro, Transient tolerance analysis of power cables thermal dynamic by interval mathematic, Electric Power System Research 77 (2007) 308–314.

[11] G. Mazzanti, Analysis of the combined effects of load cycling, thermal transients, and electrothermal stress on life expectancy of high-voltage ac cables, IEEE Transactions on Power Delivery 22 (4) (2007) 2000–2009.

[12] M. Hanna, A. Chikhani, M. Salama, Thermal analysis of power cables in multi-layered soil. part 1. theoretical model, IEEE Transactions on Power Delivery 8 (3) (1993) 761–771.

[13] C. Hwang, Calculation of thermal fields of underground cable systems with consideration of structural steels constructed in a duct bank, IEE Proceedings-Generation, Transmission and Distribution 144 (6) (1997) 541–545.

[14] J. Nahman, M. Tanaskovic, Determination of the current carrying capacity of cables using the finite element method, Electric Power Systems Research 61 (2002) 109–117.

[15] C. C. Hwang, Y. Jiang, Extensions to the finite element method for thermal analysis of underground cable systems, Electric Power Systems Research 64 (2003) 159–164.

[16] R. de Lieto Vollaro, L. Fontana, A. Vallati, Thermal analysis of underground electrical power cables buried in non-homogeneous soils, Applied Thermal Engineering 31 (2011) 772–778.

[17] C. C. Hwang, J. J. Chang, Y. H. Jiang, Analysis of electromagnetic and thermal fields for a bus duct system, Electric Power Systems Research 45 (1998) 39–45.

[18] N. Kovac, I. Sarajcev, D. Poliak, Nonlinear-coupled electric-thermal modeling of underground cable systems, IEEE Transactions on Power Delivery Vol. 21 (2006) 4–14.

[19] Guidelines for limiting exposure to time varying electric, magnetic and electromagnetic fields (up to 300 GHz), International Commission on Non-Ionizing Radiation Protection (ICNIRP) (1998).

[20] F. Freschi, L. Giaccone, M. Repetto, Educational value of the algebraic numerical methods in electromagnetism, COMPEL 27 (6) (2008) 1343–1357.

[21] M. Hanna, A. Chikhani, M. Salama, Thermal analysis of power cables in multi-layered soil. part 2. practical considerations, IEEE Transactions on Power Delivery 8 (3) (1993) 772–778.

[22] M. S. Al-Saud, M. A. El-Kady, R. D. Findlay, A new approach to underground cable performance assessment, Electric Power Systems Research 78 (2008) 907–918.

[23] J. Desmet, D. Putman, G. Vanalme, R. Belmans, D. Vandommelen, Thermal analysis of parallel underground energy cables, in: Proc. of the 18th International Conference on Electricity Distribution, Turin, 6-9 Jun 2005.

[24] A. Canova, L. Giaccone, Application of high magnetic passive loop to the magnetic mitigation of HV junction zone, in: 2nd International Conference on EMF ELF - paper 54, Paris, Mar 24-25, 2011.